Science of the Total Environment 680 (2019) 79–90

Contents lists available at ScienceDirect

Science of the Total Environment

journal homepage: www.elsevier.com/locate/scitotenv

Functional responses of smaller and larger diatoms to gradual CO_2 rise

Wei Li [a,b], Jiancheng Ding [a], Futian Li [a], Tifeng Wang [a], Yuling Yang [b], Yahe Li [a,d], Douglas A. Campbell [e], Kunshan Gao [a,c,*]

[a] State Key Laboratory of Marine Environmental Science, College of Ocean and Earth Sciences, Xiamen University, Xiamen 361102, China
[b] College of Life and Environmental Sciences, Huangshan University, Huangshan 245041, China
[c] Laboratory for Marine Ecology and Environmental Science, Qingdao National Laboratory for Marine Science and Technology, Qingdao 266071, China
[d] School of Marine Sciences, Ningbo University, Ningbo 315211, Zhejiang, China
[e] Biology Department, Mount Allison University, Sackville, NB E4L 1G7, Canada

HIGHLIGHTS

- The growth of diatoms appears to be saturated under the contemporary CO_2 level.
- A smaller diatom is more prone to photoinhibition with gradual CO_2 rise.
- CO_2 modulation methods significantly affect growth and physiological responses to CO_2.

GRAPHICAL ABSTRACT

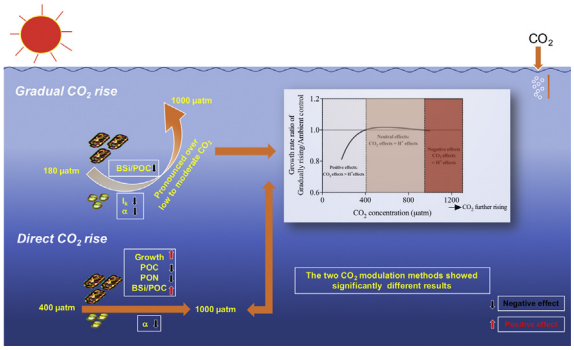

ARTICLE INFO

Article history:
Received 28 January 2019
Received in revised form 27 April 2019
Accepted 3 May 2019
Available online 05 May 2019

Editor: Jay Gan

Keywords:
Biogeochemical parameters
CO_2 modulation methods
Diatom
Growth
Ocean acidification
Photosynthetic performance

ABSTRACT

Diatoms and other phytoplankton groups are exposed to abrupt changes in pCO_2, in waters in upwelling areas, near CO_2 seeps, or during their blooms; or to more gradual pCO_2 rise through anthropogenic CO_2 emissions. Gradual CO_2 rises have, however, rarely been included in ocean acidification (OA) studies. We therefore compared how small (*Thalassiosira pseudonana*) and larger (*Thalassiosira weissflogii*) diatom cell isolates respond to gradual pCO_2 rises from 180 to 1000 μatm in steps of ~40 μatm with 5–10 generations at each step, and whether their responses to gradual pCO_2 rise differ when compared to an abrupt pCO_2 rise imposed from ambient 400 directly to 1000 μatm. Cell volume increased in *T. pseudonana* but decreased in *T. weissflogii* with an increase from low to moderate CO_2 levels, and then remained steady under yet higher CO_2 levels. Growth rates were stimulated, but Chl *a*, particulate organic carbon (POC) and cellular biogenic silica (BSi) decreased from low to moderate CO_2 levels, and then remained steady with further CO_2 rise in both species. Decreased saturation light intensity (I_k) and light use efficiency (α) with CO_2 rise in *T. pseudonana* indicate that the smaller diatom becomes more susceptible to photoinhibition. Decreased BSi/POC (Si/C) in *T. weissflogii* indicates the biogeochemical cycles of both silicon and carbon may be more affected by elevated pCO_2 in the larger diatom. The different CO_2 modulation methods resulted in different responses of some key physiological parameters. Increasing pCO_2 from 180 to

* Corresponding author at: State Key Laboratory of Marine Environmental Science, College of Ocean and Earth Sciences, Xiamen University, Xiamen 361102, China.
E-mail address: ksgao@xmu.edu.cn (K. Gao).

https://doi.org/10.1016/j.scitotenv.2019.05.035

400 μatm decreased cellular POC and BSi contents, implying that ocean acidification to date has already altered diatom contributions to carbon and silicon biogeochemical processes.

1. Introduction

The oceans are taking up over 1 million tons of CO_2 per hour derived from fossil fuel burning and changed land usage, leading to declining pH of seawater known as ocean acidification (OA) (Caldeira and Wickett, 2003; Doney et al., 2009; Sabine et al., 2004). OA threatens marine organisms and ecosystems due to altered carbonate chemistry, with increased H^+ and HCO_3^-, but decreased CO_3^{2-} and calcium carbonate saturation (Boyd, 2011; Brennan and Collins, 2015; Doney, 2006; Kroeker et al., 2013; Riebesell and Gattuso, 2015). At the same time, effects of OA under multiple environmental stressors are gaining increasing attention (Boyd et al., 2018; Xu et al., 2014). Nevertheless, inconsistent responses to OA are observed across different species and different experiment setups or at different regions (Cornwall and Hurd, 2015). Organisms may be able to acclimate to changed carbonate chemistry within short periods through plastic phenotypic changes (Sunday et al., 2014), but also through genotypic variation for long term adaptation (Collins et al., 2014; Hutchins et al., 2015; Tong et al., 2018).

While the contemporary ocean acidification rate is the fastest experienced over the last 300 million years (Hönisch et al., 2012), global average pH decline is still only about 0.002 unit per year (Solomon et al., 2007), which is much slower than abrupt pH drops applied during most OA manipulation experiments. Regionally CO_2 can indeed drop or increase rapidly due to biological production or upwelling events (Cai et al., 2011; Feely et al., 2008). To date, most OA studies abruptly shift cells to a target CO_2 level and then follow responses over short windows of 8–20 cell generations (Hennon et al., 2014; LaRoche et al., 2010) or longer windows of 100–2000 generations at the target CO_2 level (Collins et al., 2014; Hennon et al., 2014; Li et al., 2017; Lohbeck et al., 2012; Tong et al., 2018). Directly exposing organisms to a target concentration of high CO_2 without any transitional acclimation may impose an initial shock. Thus, different organisms may exhibit differential positive, balanced or negative responses during more gradually rising CO_2 and decreasing pH. The diatom *Phaeodactylum tricornutum* acclimated to short (20 generations) and longer term (1800 generations) OA showed different responses (Li et al., 2017), with smaller cell size and lower photosynthetic performance after the long term adaptation, indicating the acclimation history is critical for cells. Therefore, it is of general concern to understand how marine phytoplankton will respond to gradually rising atmosphere CO_2.

Technically, it is impracticable to truly simulate natural OA rates driven by the current CO_2 emission increase rate, even with a theoretical maximum of ca. 7 μatm increase per year, if we extrapolate from present 400 μatm to 1000 μatm by the end of this century based on the business as usual scenario (Gattuso et al., 2015). However, we can approximate natural change by gradually raising CO_2 to a target value, while tracking the progress of organism acclimation to increasing CO_2 concentrations over generational time scales. In particular we can segment change into stages from historical 180 μatm to predicted century-end 1000 μatm.

Diatoms contributed nearly one fifth of earth's primary production, playing key roles in aquatic ecosystems (Granum et al., 2005). Cell diameters of diatoms range from several μm to hundreds of μm (Finkel et al., 2010) and the responses of growth, photosynthesis, sinking rate, and affinity for nutrients under changed environmental conditions are all size-dependent (Finkel et al., 2010; Key et al., 2010; Richier et al., 2018; Sarthou et al., 2005; Wu et al., 2014a). Although numerous studies have detailed positive, negative or neutral responses to OA in growth, photosynthetic and biogeochemical properties, the effects of OA on diatoms are still uncertain (Gao and Campbell, 2014). The aim of this study is to compare and clarify the CO_2 effects of gradually vs. directly increasing CO_2, by gradually increasing CO_2 from a glacial level of 180 μatm to the 1000 μatm that is expected for the year of 2100; or by directly exposing cells from the current CO_2 level of 400 μm to 1000 μm, using both a small diatom *Thalassiosira pseudonana* (CCMP1335) and a larger diatom *Thalassiosira weissflogii* (CCMA 102), which have both been used in OA ecophysiological studies (Gao et al., 2012a; Hennon et al., 2014; Hopkinson et al., 2011). Their morphological, physiological and biogeochemical properties were then tracked over multiple generations. Our study provides new insights into ocean acidification simulation methods and the differential responses of diatom species with different cell sizes to a more realistically approximated CO_2 change scenario.

2. Materials and methods

2.1. Algae culture and pCO_2 treatments

Thalassiosira pseudonana (CCMA 102) and *Thalassiosira weissflogii* (CCMP1336) were obtained from microalgal collections of the State Key Laboratory of Marine Environmental Science at Xiamen University. Both strains were cultured under 20 °C at a light intensity of 220 μmol m^{-2} s^{-1} with light dark cycle of 12:12. Artificial seawater was used and enriched with modified Aquil medium (Morel et al., 1979) with NO_3^-, PO_4^{3-} and SiO_3^{2-} adjusted to 20 μmol L^{-1}, 2 μmol L^{-1} and 20 μmol L^{-1}, respectively. Cells were grown under ambient CO_2 before subsequent transfer. The seawater carbonate chemistry in cultures was manipulated through additions of HCO_3^- ($NaHCO_3$) or HCl in a closed system according to Gattuso et al. (2010), and concentrations of dissolved inorganic carbon (DIC) at different pCO_2 levels were estimated using CO_2SYS (Pelletier et al., 2007) (Supplementary Table S1). The increase of pCO_2 level from 180 μatm to 1000 μatm was divided into 22 steps with an interval of 40 μatm, except for an interval of 20 μatm from 380 to 400 μatm (Fig. 1a). The initiating 180 μatm grown cells were transferred from ambient 400 μatm and acclimated for ca. 10–20 generations before being used in the gradually rising CO_2 study. Cells were inoculated at an initial concentration of ca. 50–150 cells mL^{-1} under each pCO_2 level for both species and were then grown for 4–5 days allowing the cultures to attain ca. $5 * 10^4$ cells mL^{-1} for *T. pseudonana* and ca. $0.9 * 10^4$ cells mL^{-1} for *T. weissflogii*. These fairly low cell densities allowed us to maintain the pH within minor variations (ca. <0.05 units) compared with set pH values (Supplementary Table S2). Cells were thus acclimated for ca. 8–10 generations in *T. pseudonana* or ca. 5–7 generations in *T. weissflogii* under each CO_2 level. Cells incubated under a CO_2 level for 4–5 days were then diluted into a higher CO_2 concentration, with each treatment given 3 biological replicate cultures. The cultures thus went through cumulatively ca. 195 generations in *T. pseudonana* and ca. 145 generations in *T. weissflogii* before reaching 1000 μatm (Fig. 1b). During the whole experiment, parallel cell cultures were concurrently semi-continuously cultured at 400 μatm as a control treatment. After the gradually rising CO_2 study, cells grown at 400 μatm (control treatment) were inoculated directly into high CO_2 of 1000 μatm and then acclimated for ca. 20 generations in *T. pseudonana* or ca. 12 generations in *T. weissflogii* (Fig. 1c, d), to compare effects of the high CO_2 (1000 μatm vs. 400 μatm) and the modulation methods of gradual vs. direct. The ambient control of direct increase CO_2 continued from the ambient control of gradual modulation method. The pH of cultures was measured at the end of each CO_2 level with a pH probe (Mettler Toledo DL15 Titrator, Sweden) which was calibrated with NBS buffer solutions each time before using.

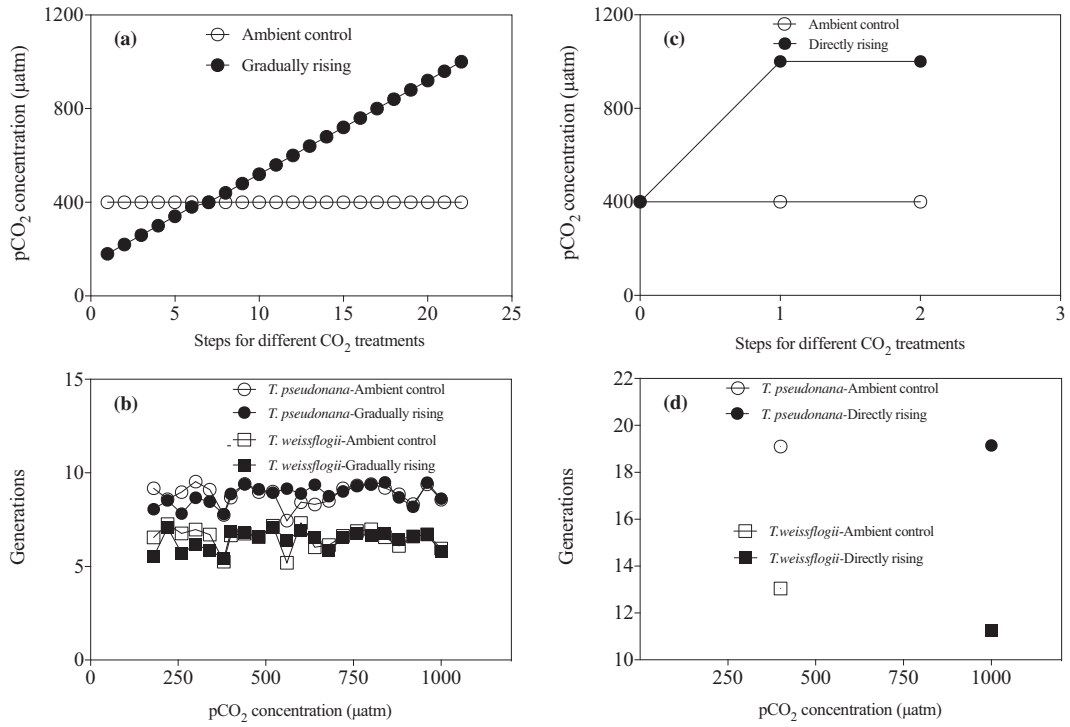

Fig. 1. The experimental design for the CO_2 treatments with gradually rising CO_2 from 180 μatm to 1000 μatm at intervals of ca. 40 μatm (except an interval of 20 μatm from 380 to 400 μatm) with 4–5 days culture at each step (a). Cells grew through ca.195 generations for *Thalassiosira pseudonana* and ca.145 generations for *Thalassiosira weissflogii* (b) before reaching 1000 μatm. The experimental design for a direct increase in CO_2 from 400 μatm to 1000 μatm (c) with cells acclimated ca.20 generations under 1000 μatm for *T. pseudonana* and ca.12 generations for *T. weissflogii* (d).

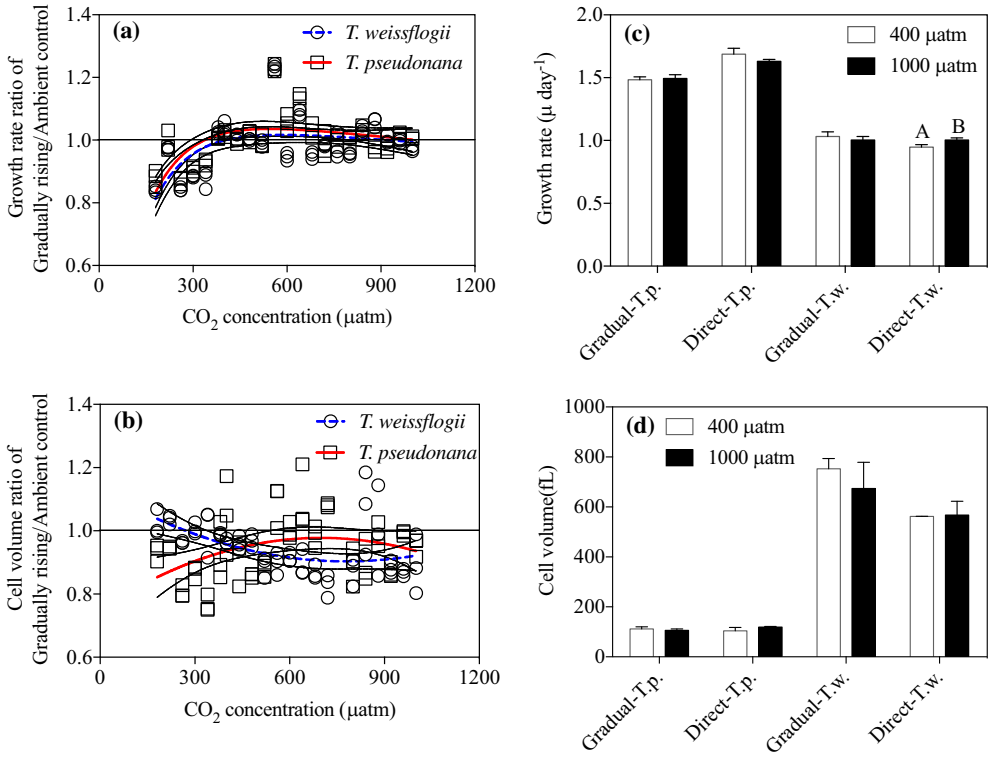

Fig. 2. The specific growth rate ratio (a) and cell volume ratio (b) in *Thalassiosira pseudonana* (T.p.) and *Thalassiosira weissflogii* (T.w.) of gradually rising CO_2 to ambient control (continuously grown under 400 μatm), and the specific growth rates (c) and cell volume (d) under 400 μatm and 1000 μatm with gradually rising (indicated as Gradual-T.p. or Gradual-T.w.) or directly rising (indicated as Direct-T.p. or Direct-T.w.) CO_2. The growth rate and cell volume were measured in the middle of the light phase. The growth rate ratio from 180 μatm to 1000 μatm of *T. pseudonana* (open square, solid curve fit) and *T. weissflogii* (open circle, dashed curve fit) were fit with an equation from Platt et al. (1980): $\mu_{gradual}/\mu_{ambient}=(\mu_{gradual}/\mu_{ambient})_{max}*(1-e^{(-\alpha*CO_2/(\mu_{gradual}/\mu_{ambient})_{max})})*e^{(-\beta*CO_2/(\mu_{gradual}/\mu_{ambient})_{max})}$. Cell volume ratio from 180 μatm to 1000 μatm of *T. pseudonana* (open square, solid curve fit) and *T. weissflogii* (open circle, dashed curve fit) were fit with a centered second order polynomial (quadratic) model, the dotted lines show 95% confidence intervals. Different letters indicate significant difference between CO_2 treatments at $p < 0.05$ level; bars without labeling indicate no significant difference between CO_2 treatments.

2.2. Growth rate and cell volume measurements

Growth rates of both *T. pseudonana* and *T. weissflogii* were calculated according to:

$$\mu = (\ln(\text{Cell } T_{final}) - \ln(\text{Cell } T_0))/t$$

where Cell T_{final} is the cell suspension density at the end of each incubation and Cell T_0 is the initial cell concentration, while "t" is the time elapsed during the culture step or between two consecutive dilutions. Cell suspension density and cell volume were determined with a Z2™ Coulter Counter (Beckman, Buckinghamshire, UK). The growth rate ratio of gradually rising CO_2 growth rate ($\mu_{gradual}$) divided by ambient control growth rate ($\mu_{ambient}$) was fit as a function of CO_2 levels using an equation from Platt et al. (1980):

$$\mu_{gradual}/\mu_{ambient} = \left(\mu_{gradual}/\mu_{ambient}\right)_{max} * \left(1 - e^{\left(-\alpha * CO_2/\left(\mu_{gradual}/\mu_{ambient}\right)_{max}\right)}\right) * e^{\left(-\beta * CO_2/\left(\mu_{gradual}/\mu_{ambient}\right)_{max}\right)}$$

where $\mu_{gradual}/\mu_{ambient}$ is the instantaneous growth rate ratio; $(\mu_{gradual}/\mu_{ambient})_{max}$ is the maximum growth rate ratio; α is the initial slope of growth rate ratio; and β is the inhibition parameter of growth rate ratio.

2.3. Pigment measurement

To determine chlorophyll *a* (Chl *a*) and carotenoid content, cells were filtered onto GF/F filters and extracted with absolute methanol at 4 °C over night. The extracts were centrifuged at 5000*g* for 10 min under 4 °C (Universal 320R, Hettich, Germany) and then scanned with a spectrophotometer (DU800, Beckman, Fullerton, California, USA). Chl *a* and carotenoid were then estimated according to following Ryckebosch et al. (2011) which was modified from Wellburn (1994).

2.4. Photosynthetic performance measurement

To determine photosynthetic performance time inductions and rapid light curves (RLC) of chlorophyll fluorescence parameters were determined with a Xe-PAM (Walz, Germany) for all CO_2 levels except 560, 680 and 960 μatm which were omitted because of technical problems. For the induction curves the actinic light was set at 156 μmol m^{-2} s^{-1} and each saturation pulse was set at 5000 μmol photons m^{-2} s^{-1} for 0.8 s. RLC were measured at 8 actinic light levels of 0, 76 or 156, 226, 337, 533, 781, 1077, 1593 and 2130 or 2854 μmol m^{-2} s^{-1} with saturation pulses of 5000 μmol photons m^{-2} s^{-1} for 0.8 s, at an interval of 10 s between each actinic light. The maximum quantum yield (F_V/F_M) and effective quantum yield of PSII (Φ_{PSII}) were calculated following Genty et al. (1990):

$$F_V/F_M = (F_M - F_0)/F_M;$$

$$\Phi_{PSII} = (F_M' - F_t)/F_M';$$

Non-photochemical quenching (NPQ) was calculated using:

$$NPQ = (F_M - F_M')/F_M'$$

where F_M and F_0 indicate the maximum and minimum fluorescence yield after 15 min dark adaptation, F_M' indicates the light-adapted maximal chlorophyll fluorescence yield, and F_t is the steady fluorescence level during the exposures.

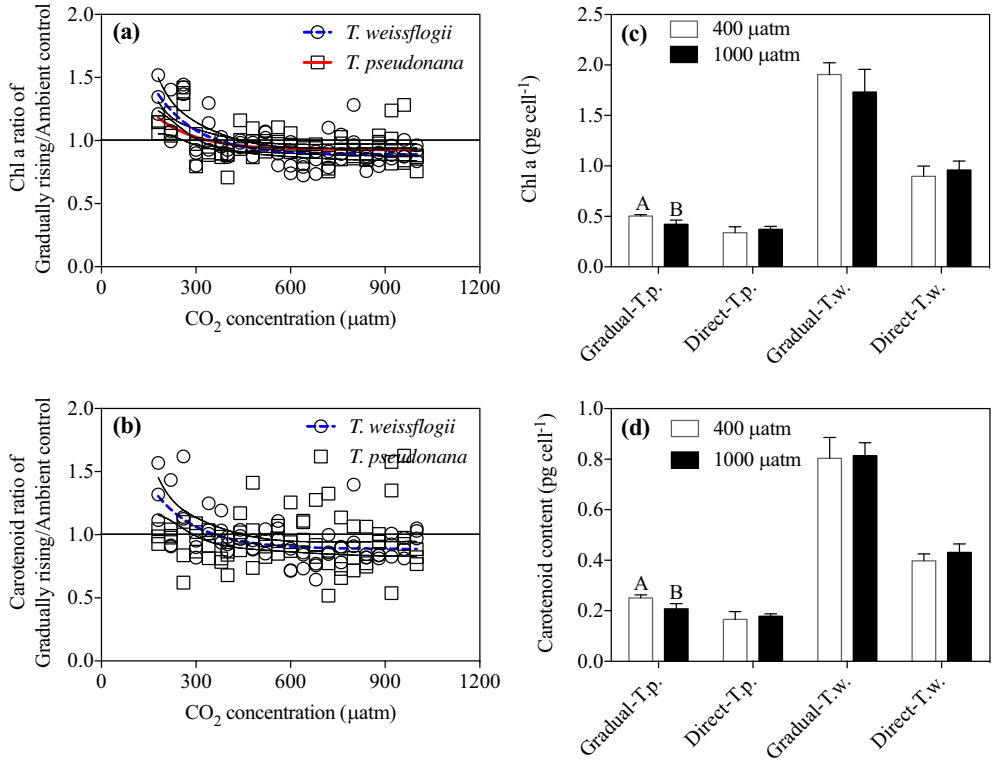

Fig. 3. The Chl *a* (a) and carotenoid (b) ratio of gradually rising CO_2 to ambient control (continuously grown under 400 μatm), and the contents of Chl *a* (c) and carotenoid (d) under 400 μatm and 1000 μatm with gradually rising (indicated as Gradual-T.p. or Gradual-T.w.) and directly rising CO_2 (indicated as Direct-T.p. or Direct-T.w.) in *Thalassiosira pseudonana* and *Thalassiosira weissflogii*. Samples for pigment measurement were collected in the middle of light phase. The Chl *a* ratio as a function of CO_2 concentration in *T. pseudonana* (open square, solid curve fit) and *T. weissflogii* (open circle, dashed curve fit) and carotenoid ratio as a function of CO_2 concentration in *T. weissflogii* (open circle, dashed curve fit) were fit with an exponential decay model: $Y = (Y_0 - \text{plateau}) * e^{(-k*x)} + \text{plateau}$, the dotted lines show 95% confidence intervals. Different letters indicate significant difference between CO_2 treatments at $p < 0.05$ level; bars without labeling indicate no significant difference between CO_2 treatments.

Relative electron transport rate (rETR) was calculated according to equation:

$$rETR = \Phi_{PSII} \times 0.5 \times PFD$$

where PFD indicates the intensity of actinic light level. Relative maximum electron transport rate ($rETR_{max}$), light use efficiency (α) and saturation light intensity (I_k) were acquired from RLC of rETR, fit according to Webb et al. (1974).

2.5. Carbon fixation rate measurement

A ^{14}C method was used for carbon fixation rate measurements (Nielsen, 1952) for all CO_2 levels except 260 μatm and 960 μatm which were omitted because of technical problems. Briefly, *T. pseudonana* and *T. weissflogii* grown under different treatments were sampled to 20 mL glass scintillation tubes (Perkin Elmer) and injected with 100 μL-5 μCi (0.185 MBq) $NaH^{14}CO_3$ solution (ICN Radiochemicals), with another two tubes wrapped with aluminum foil as a dark control. Cells incubated under culture light intensity of 220 μmol m^{-2} s^{-1} for 1 h were then filtered onto Whatman GF/F glass filters. Then, filters were transferred into 20 mL scintillation vials, fumed with HCl (12 mol L^{-1}) for 12 h to expel the non-fixed inorganic carbon as CO_2 and then dried in an oven for 6 h at 45 °C. 5 ml of scintillation cocktail (Tri-Carb 2800TR, Perkin Elmer®) was added to the vials, which were then counted with a liquid scintillation counter (LS 6500, Beckman Coulter, USA). Calculation of carbon fixation rates normalized to per cell was as detailed in Li et al. (2015).

2.6. Particulate organic carbon (POC) and particulate organic nitrogen (PON) measurements

To determine the POC and PON contents of *T. pseudonana* and *T. weissflogii* cultured at different pCO_2 levels, cells were collected at mid light period and filtered onto Whatman GF/F filters that were precombusted at 450 °C for 6 h before use. Collections were fumed with

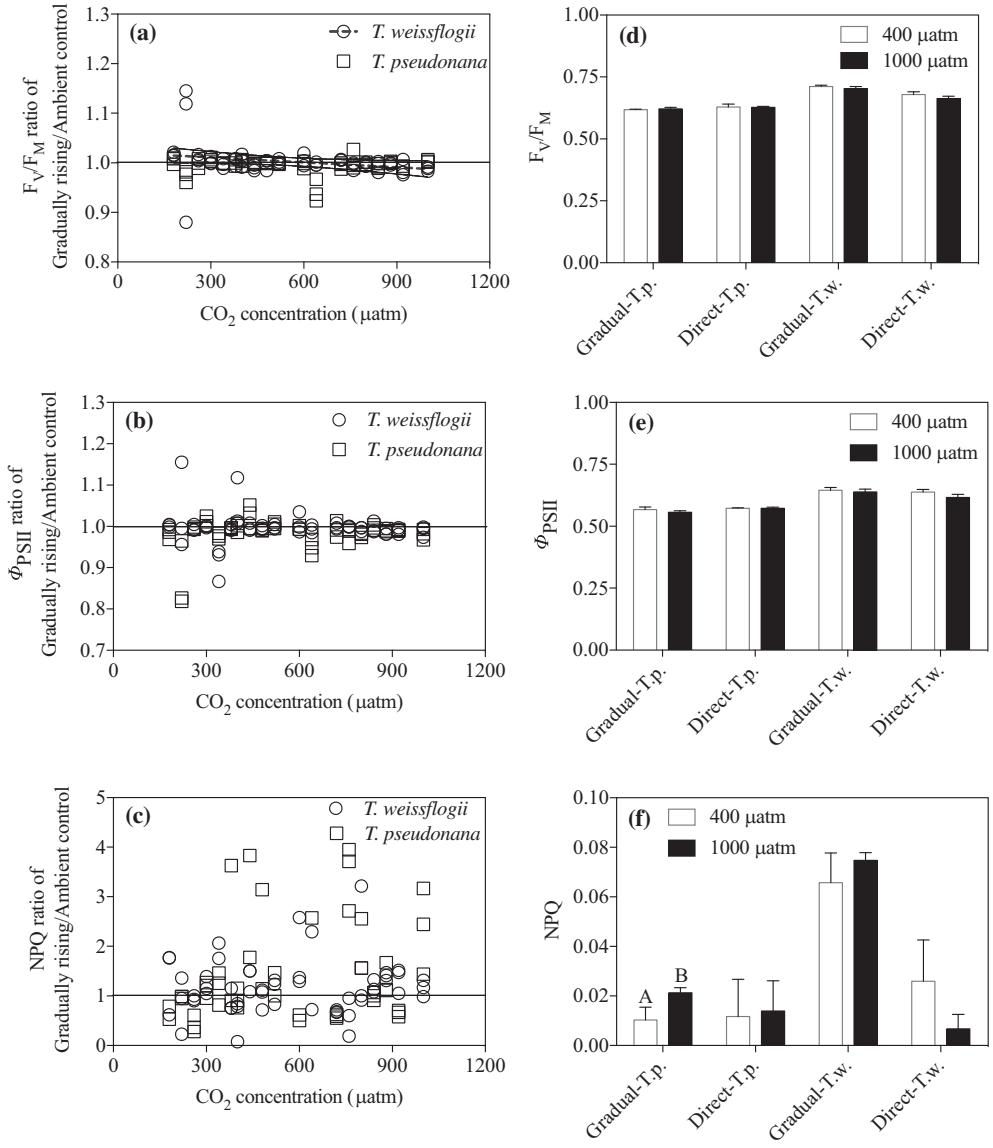

Fig. 4. The F_V/F_M (a), Φ_{PSII} (b) and NPQ (c) ratios of gradually rising CO_2 to ambient control (continuously grown under 400 μatm), and the F_V/F_M (d), Φ_{PSII} (e) and NPQ (f) under 400 μatm and 1000 μatm with gradually rising (indicated as Gradual-T.p. or Gradual-T.w.) and directly rising (indicated as Direct-T.p. or Direct-T.w.) CO_2 in *Thalassiosira pseudonana* and *Thalassiosira weissflogii*. The F_V/F_M, Φ_{PSII} and NPQ were measured in the middle of light phase. F_V/F_M ratio as a function of CO_2 concentration in *T. weissflogii* (open circle, dashed curve fit) was fit with a linear regression model, the dotted lines showed 95% confidence intervals. Different letters indicate significant difference between CO_2 treatments at $p < 0.05$ level; bars without labeling indicate no significant difference between CO_2 treatments.

HCl (12 mol L^{-1}) for 12 h and then dried in an oven at 60 °C for another 12 h. A PerkinElmer Series II CHNS/O Analyzer 2400 was used for carbon and nitrogen measurements.

2.7. Cellular biogenic silica (BSi) measurement

Cells cultured under different conditions were collected onto Polycarbonate Membrane Filters (Millipore, 0.22 μm), dried in an oven for 12 h and then measured with a spectrophotometric method according to Brzezinski and Nelson (1995).

2.8. Statistical analysis

The relationship between gradually rising CO_2 levels and the corresponding parameters were determined with a curve fit of either an exponential decay model or a polynomial curve, using the ratio of experimental CO_2 treatment to the ambient control (400 μatm) as "Y" axis, and with CO_2 concentration as "X" axis. An unpaired *t*-test was used to establish differences between 400 μatm and 1000 μatm in gradually and directly rising CO_2 methods at a confidence level of 95%, using Prism 7.0 software.

3. Results

3.1. Growth rate and cell volume

The growth rates of both *T. pseudonana* and *T. weissflogii* were stimulated by a CO_2 rise from low to moderate levels but then stabilized with further CO_2 rise (Fig. 2a), at a maximum fitted growth rate ratio of gradually rising to ambient control $(\mu_{gradual} / \mu_{ambient})_{max}$ of 1.07 for

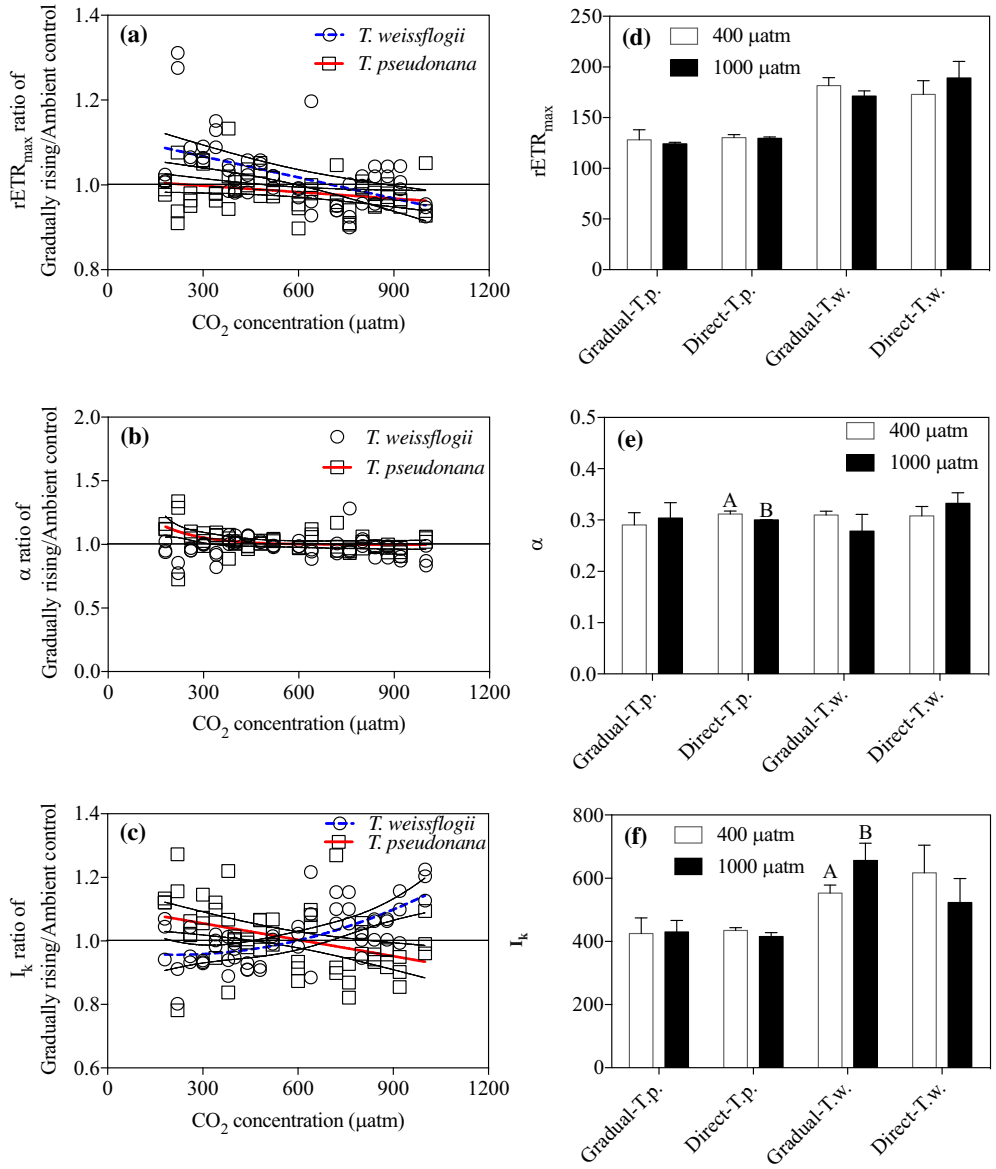

Fig. 5. The $rETR_{max}$ (a), α (b) and I_k (c) ratios of gradually rising CO_2 to ambient control (continuously grown under 400 μatm), and the $rETR_{max}$ (d), α (e) and I_k (f) under 400 μatm and 1000 μatm with gradually rising (indicated as Gradual-T.p. or Gradual-T.w.) and directly rising CO_2 (indicated as Direct-T.p. or Direct-T.w.) in *Thalassiosira pseudonana* and *Thalassiosira weissflogii*. The rapid light curve was measured in the middle of light phase. $rETR_{max}$ ratio as a function of CO_2 concentration in *T. pseudonana* (open square, solid curve fit) and *T. weissflogii* (open circle, dashed curve fit) were fit with a linear regression model; α ratio as a function of CO_2 concentration in *T. pseudonana* (open square, solid curve fit) was fit with an exponential decay model; I_k ratio as a function of CO_2 concentration in *T. pseudonana* (open square, solid curve fit) and *T. weissflogii* (open circle, dashed curve fit) were fit with linear regression model and centered second order polynomial (quadratic) models, respectively. Dotted lines showed 95% confidence intervals. Different letters indicate significant difference between CO_2 treatments at $p < 0.05$ level; bars without labeling indicate no significant difference between CO_2 treatments.

T. pseudonana and 1.11 for *T. weissflogii*. The cell volume showed an increasing trend in the small cells of *T. pseudonana*, but showed a decreasing trend in the larger cells of *T. weissflogii* from low to moderate CO_2 levels, and was then steady under yet higher CO_2 levels (Fig. 2b). There were no significant effects of high CO_2 (1000 μatm) upon the growth rate and cell volume when compared to the ambient control under the two modulation methods (unpaired *t*-test, df = 4, all $p > 0.05$) (Fig. 2c, d), except that directly rising CO_2 to 1000 μatm stimulated the growth rate by 5.8% in *T. weissflogii* compared to the ambient control (unpaired t-test, $t = 3.778$, df = 4, $p = 0.02$).

3.2. Pigmentation

Chl *a* declined as CO_2 rose from low to moderate levels and was then steady under yet higher CO_2 levels in both species (Fig. 3a). For carotenoids this trend was observed only in *T. weissflogii* (Fig. 3b). There were no significant effects of high CO_2 (1000 μatm) on Chl *a* and carotenoid contents when compared to the ambient control under the two modulation methods (unpaired *t*-test, df = 4, all $p > 0.05$) (Fig. 3c, d), except that in *T. pseudonana* gradually rising CO_2 under 1000 μatm decrease the Chl *a* and carotenoid by 16.39% (unpaired *t*-test, $t = 3.231$, df = 4, $p = 0.03$) and 17.35% (unpaired t-test, $t = 3.136$, df = 4, $p = 0.04$) (Fig. 3c, d).

3.3. Photosynthetic performance

Gradually rising CO_2 did not affect the F_V/F_M of *T. pseudonana* (linear regression, $p = 0.83$) (Fig. 4a), but F_V/F_M decreased with gradually rising CO_2 in *T. weissflogii* (linear regression, $R^2 = 0.07$, $p = 0.046$) (Fig. 4a). Gradually rising CO_2 did not affect the effective quantum yield (Φ_{PSII}) (linear regression, $p = 0.31$, *T. pseudonana* or 0.54, *T. weissflogii*) nor NPQ (linear regression, $p = 0.50$, *T. pseudonana* or 0.11, *T. weissflogii*) (Fig. 4b, c). There were no significant effects of high CO_2 (1000 μatm) on F_V/F_M, Φ_{PSII} and NPQ compared to the ambient control (400 μatm) under the two modulation methods (unpaired *t*-test, df = 4, all $p > 0.05$) (Fig. 4d, e, f), except that NPQ was increased by 106.5% at 1000 μatm in *T. pseudonana* with gradually rising of CO_2 (unpaired t-test, $t = 3.44$, df = 4, $p = 0.03$) (Fig. 4f).

$rETR_{max}$ showed a negative relationship with gradually rising CO_2 in both species (linear regression, $p < 0.0001$ in *T. pseudonana*; $p = 0.04$ in *T. weissflogii*) (Fig. 5a). Light use efficiency (α) declined from low to moderate CO_2 levels and was then steady under higher CO_2 levels in *T. pseudonana* (Fig. 5b). Saturation light intensity (I_k) declined with rising CO_2 in *T. pseudonana* (linear regression, $p = 0.001$), but showed an increase in *T. weissflogii* from low to high CO_2 levels (Fig. 5c). There was no significant effects of high CO_2 (1000 μatm) on $rETR_{max}$ when compared to the ambient control (400 μatm) under the two modulation methods (unpaired *t*-test, df = 4, all $p > 0.05$) (Fig. 5d), however the α in *T. pseudonana* decreased by 3.8% in cells grown under directly increased CO_2 (unpaired t-test, $t = 3.539$, df = 4, $p = 0.02$) (Fig. 5e), and I_k increased by 18.6% was in gradually rising CO_2 treatment in *T. weissflogii* at 1000 μatm (unpaired t-test, $t = 2.975$ df = 4, $p = 0.04$) (Fig. 5f).

3.4. Carbon fixation rate

Neither gradually rising CO_2 (linear regression, $p = 0.07$) nor the comparison of the ambient control to 1000 μatm in the two CO_2 modulation methods significantly affected the carbon fixation rate in *T. pseudonana* (unpaired *t*-test, df = 4, all $p > 0.05$) (Fig. 6a, b). However, carbon fixation rate showed a negative relationship with gradually rising CO_2 in *T. weissflogii* (Fig. 6a), where it also decreased by 34.6% under 1000 μatm compared with the ambient control (400 μatm) (unpaired t-test, $t = 3.071$, df = 4, $p = 0.04$) (Fig. 6b).

3.5. Particulate organic carbon and nitrogen

Particulate organic carbon (POC) declined from low to moderate CO_2 levels and was then steady under higher CO_2 levels in both *T. pseudonana* and *T. weissflogii* (Fig. 7a), with no significant patterns of particulate organic nitrogen (PON) in either species (Fig. 7b). C/N thus showed a negative relationship in *T. pseudonana* from low to moderate CO_2 levels and then kept steady under higher CO_2 levels, and declined with CO_2 levels in *T. weissflogii* (linear regression, $R^2 = 0.11$, $p = 0.008$) (Fig. 7c). POC and PON were significantly decreased by 20.8% (unpaired t-test, $t = 3.649$, df = 4, $p = 0.02$) and 17.2% (unpaired t-test, $t = 4.708$, df = 4, $p = 0.009$) respectively in *T. weissflogii* cells under a direct rise in CO_2 to 1000 μatm (Fig. 7d, e), but not in cells under the gradually rising CO_2 treatment (unpaired t-test, df = 4, all $p > 0.05$). There was no significant difference of C/N between 400 μatm and 1000 μatm in the two modulation methods (unpaired t-test, df = 4, all $p > 0.05$) (Fig. 7f).

3.6. Cellular biogenic silica (BSi) and ratio of BSi to POC(Si/C)

Gradually rising CO_2 decreased the cellular biogenic silica (BSi) contents of both *T. pseudonana* and *T. weissflogii* from low to moderate CO_2 levels, which were then steady with higher CO_2 (Fig. 8a). The Si/C only decreased from low to moderate CO_2 levels and was then steady with higher CO_2 levels in the larger *T. weissflogii* (Fig. 8b). No significant difference of BSi was detected when comparing the ambient control (400 μatm) with their 1000 μatm treatments under either modulation method (unpaired t-test, df = 4, all $p > 0.05$) (Fig. 8c). The BSi/C was increased by 20.7% in *T. weissflogii* in cells under a direct increase of CO_2 to 1000 μatm (unpaired t-test, $t = 14.33$, df = 4, $p = 0.0001$) (Fig. 8d).

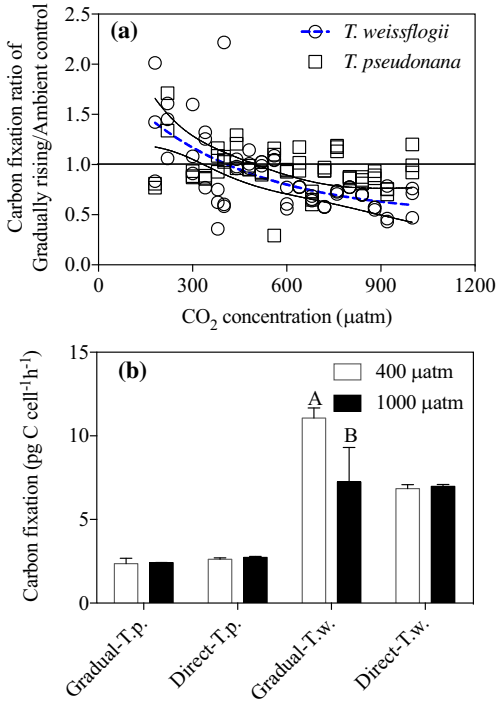

Fig. 6. The carbon fixation rate (a) ratio of gradually rising CO_2 to ambient control (continuously grown under 400 μatm), and the carbon fixation rate per cell (b) under 400 μatm and 1000 μatm with gradually rising (indicated as Gradual-T.p. or Gradual-T.w.) and directly rising CO_2 (indicated as Direct-T.p. or Direct-T.w.) in *Thalassiosira pseudonana* and *Thalassiosira weissflogii*. Carbon fixation rates were measured in the middle of light phase. Carbon fixation rate ratio as a function of CO_2 concentration in *T. weissflogii* (open circle, dashed curve fit) was fit with an exponential decay model, the dotted lines showed 95% confidence intervals. Different letters indicate significant difference between CO_2 treatments at $p < 0.05$ level; bars without labeling indicate no significant difference between CO_2 treatments.

The decrease in the BSi/C ratio between gradually rising CO_2 to ambient control is explicable as a secondary effect of the response of growth rate to gradually rising CO_2 to ambient control in both *Thalassiosira pseudonana* and *Thalassiosira weissflogii* (Fig. 9).

4. Discussion

Marine phytoplankton have shown varied responses to OA effects across studies using a direct shift to the target CO_2 concentrations. In this study we tested how organisms respond to gradually rising CO_2 and compared whether cell responses differ under gradual vs. direct increases in CO_2. The differential effects of gradually rising CO_2 vs. directly rising CO_2 were more pronounced from low to moderate CO_2 levels. OA effects then differed a lot whether achieved by gradual or direct modulation from the ambient control (400 μatm) to measures under high CO_2 of 1000 μatm.

Short-term and longer-term acclimation periods induce different responses in physiological traits under OA (Jin et al., 2013; Li et al., 2017). Genetic adaptation to OA may happen within a few hundred generations (Lohbeck et al., 2012; Schaum et al., 2013). In the present study, growth rates of both small (*T. pseudonana*) and larger (*T. weissflogii*) diatoms increased under long term acclimation to gradually rising CO_2 over the pCO_2 range from low to moderate levels (Fig. 2a), but then kept steady as CO_2 rose further to yet higher future levels. This indicates that any growth promotion of OA upon field populations of these diatoms has likely already saturated. Cell growth can benefit from increased CO_2 supply, especially when starting from the lower level of glacial CO_2 concentration (180 μatm), through down regulation of the energy cost of carbon concentrating mechanisms (CCMs) (Reinfelder, 2011). However, the simultaneous increase in H^+ also increases the energy cost for the intra-cellular acid base balance modulation (Gao and Campbell, 2014), and energy flux may re-allocate between CCMs and photorespiration (Gao et al., 2012b; Hennon et al., 2017).

Rising CO_2 and H^+ concentrations thus affect the physiological performances of phytoplankton differentially (Goldman et al., 2017; Wu et al., 2017). Leaving aside other co-varying factors of light, temperature and

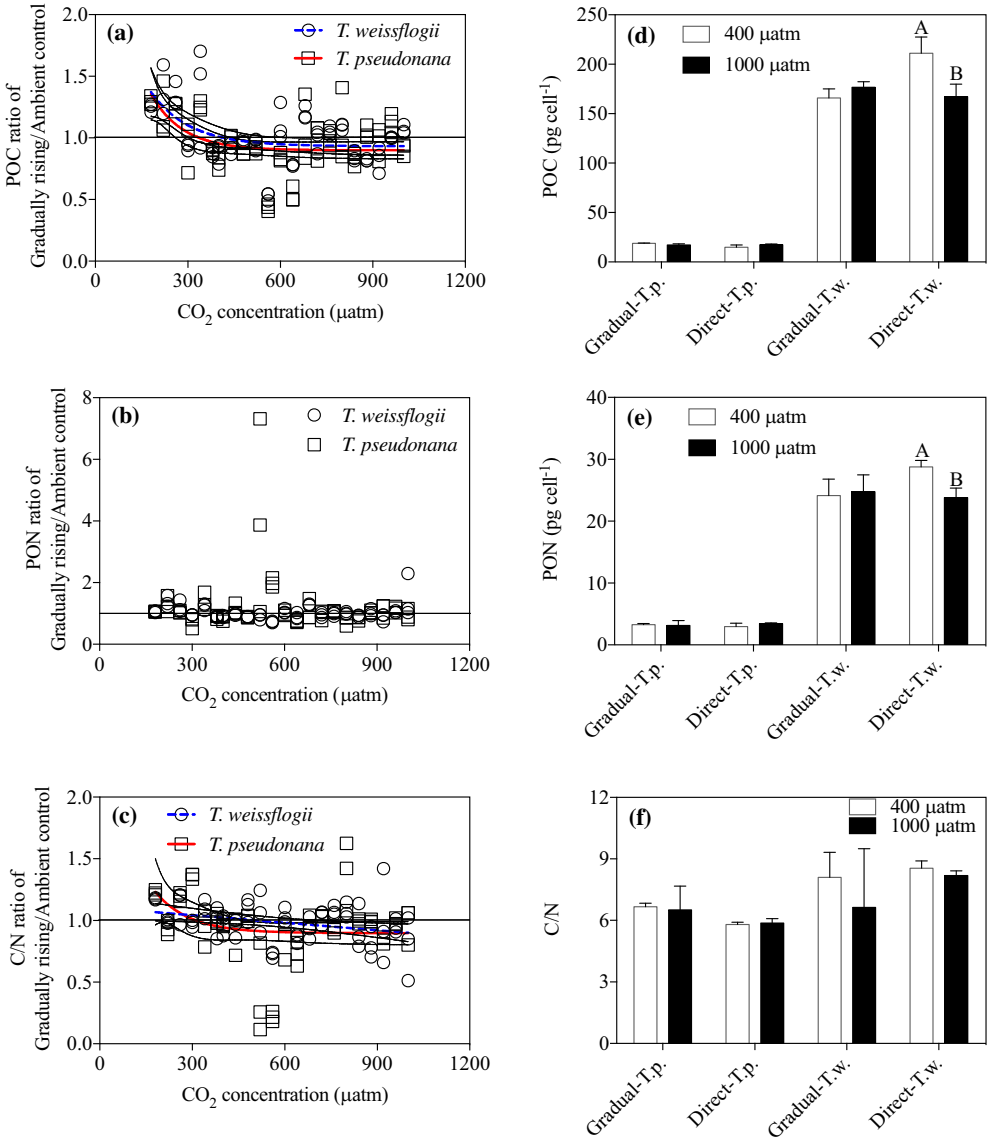

Fig. 7. The POC (a), PON (b) and C/N (c) ratio of gradually rising CO_2 to ambient control (continuously grown under 400 μatm), and the contents of POC (d), PON (e) and C/N (f) under 400 μatm and 1000 μatm with gradually rising (indicated as Gradual-T.p. or Gradual-T.w.) and directly rising CO_2 (indicated as Direct-T.p. or Direct-T.w.) in *Thalassiosira pseudonana* and *Thalassiosira weissflogii*. Samples for POC, PON measurement were collected in the middle of light phase. POC ratio as a function of CO_2 concentration in *T. pseudonana* (open square, solid curve fit) and *T. weissflogii* (open circle, dashed curve fit) were fit with an exponential decay model; C/N ratio as a function of CO_2 concentration in *T. pseudonana* (open square, solid curve fit) and *T. weissflogii* (open circle, dashed curve fit) were fit with an exponential decay model or linear regression model, respectively. Dotted lines showed 95% confidence intervals. Different letters indicate significant difference between CO_2 treatments at $p < 0.05$ level; bars without labeling indicate no significant difference between CO_2 treatments.

nutrient regimes (Gao et al., 2017; Li et al., 2017), the balance between increased dissolved CO_2 and HCO_3^- with increased H^+ concentration is likely key to determine net primary production responses to OA. Based on our present results, we hypothesize that rising CO_2 will lead to a compensation range or tipping point between the positive effects of increased CO_2, which have been largely realized already, and the negative effects of enhanced H^+ concentration, which will dominate the effects of OA at future pCO_2 levels (Fig. 10). The positive, neutral and negative effects of CO_2 concentration range or tipping point may be species-specific or even population-specific (Zhang et al., 2018), and they also may be mediated by other co-variants (Listmann et al., 2016; Sett et al., 2014). Therefore, to predict the growth-related responses to increased CO_2 and decreased H^+, more taxa or source niches should be considered.

Cell volume can be mediated by many environmental and physiological factors (Parsons and Takahashi, 1973), such as light intensity (Thompson et al., 1991) and nutrient condition (Li et al., 2012). Differential cell volume responses of the smaller vs. larger species indicate species- or size-specific responses in physiological adjustment and carbon expenditure strategies as a response to OA (Collins et al., 2014; F. Li et al., 2017). Although the cell volume of *T. pseudonana* increased from low to moderate CO_2 levels the averaged cell volume ratio of gradually rising CO_2 to ambient control remained <1 (Fig. 2b).

Smaller cell volume together with attenuation of the frustule (see below) may mitigate CO_2 diffusion limitations through enhancement of surface area to volume ratio, and thus stimulate cell growth (Flynn et al., 2012). On the other hand, CO_2 diffusion rate and pH buffer capacities around the cellular diffusive boundary layer vary with cell size and may have co-varying differences with cellular metabolic rates (Flynn et al., 2012). While larger diatom cells may benefit from elevated CO_2 (Wu et al., 2014b), larger cells may require more energy to cope with larger pH drop around the cellular diffusive boundary layer during night period, together with enhanced mitochondrial respiration or photorespiration under lower pH (Gao et al., 2012a; Wu et al., 2010; Yang and Gao, 2012) resulting in decreased carbon fixation rates in the larger cell in the present work.

Therefore, differently sized cells have different responses to rising dissolved pCO_2 (Finkel et al., 2010; Flynn et al., 2012), that may be modulated by other environmental drivers (Boyd et al., 2018). Light is a key interacting factor influencing diatoms' responses to rising CO_2 (Gao et al., 2012b; Ihnken et al., 2011; Li and Campbell, 2013; Li et al., 2017). Larger diatom cells are known to have lower intrinsic susceptibility to photoinactivation of photosystem II compared with the smaller cells (Key et al., 2010). In the present work, smaller cell volume of *T. pseudonana* showed higher susceptibility to light as evidenced by decreased pigmentation (Fig. 3a, b) and lowered $rETR_{ax}$ (Fig. 5a), α (Fig. 5b) and I_k (5c). Cell size scaling responses related to light may be further amplified with predicted shoaling of the upper mixed layer in future oceans, which increases daytime integrated solar exposures to the cells within this layer (Capotondi et al., 2012; Gao et al., 2012a).

Diatoms are one of the largest silicifying contributors to biogeochemical cycles of silicon (Si) due to their siliceous wall (Tréguer and De La Rocha, 2013). The siliceous cell wall of diatoms may be important in pH buffering for the activity of carbonic anhydrase enzyme (Milligan and Morel, 2002); and decreased biogenic silicate content in diatoms due to OA were found in other studies (Mejía et al., 2013; Tatters et al., 2012). Therefore, diatoms may suffer indirectly from OA due to reduced silification, and acclimate to changed carbonate chemistry during gradually rising CO_2 (Sunday et al., 2014).

Gradually increasing CO_2 from 180 to 400 μatm significantly decreased biogenic silicate contents of both diatoms, while further increase in the CO_2 partial pressure above 400 μatm had little further impact on biogenic silicate. The decreased biogenic silicate contents

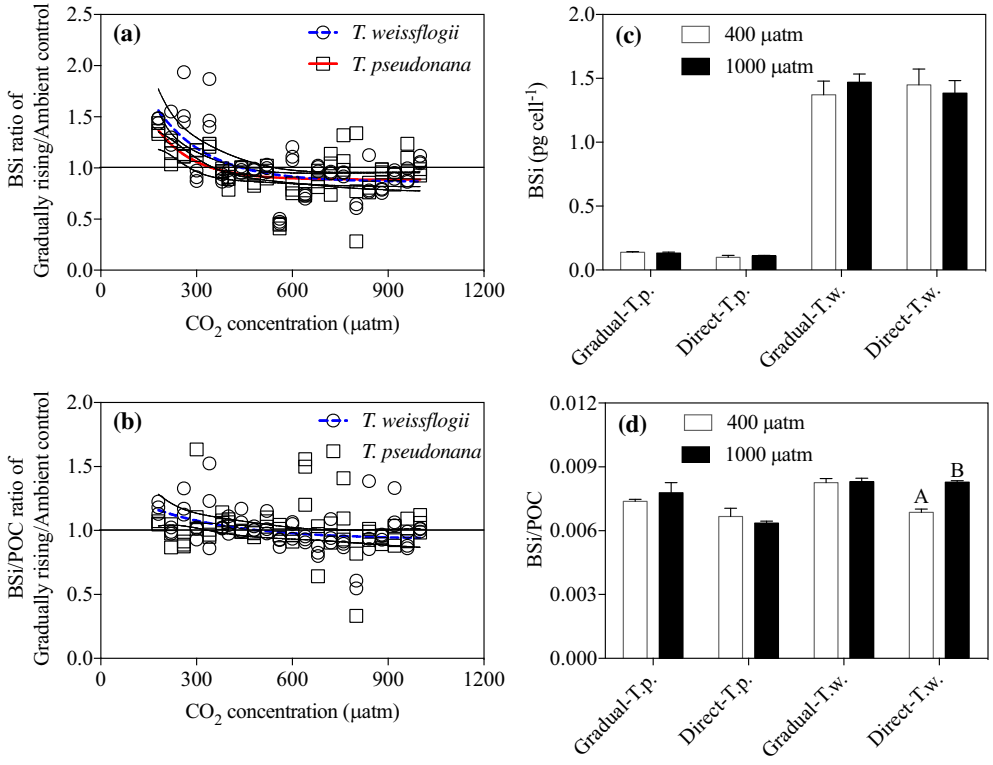

Fig. 8. The biological silicon (BSi) (a) and BSi/POC (b) ratio of gradually rising CO_2 to ambient control (continuously grown under 400 μatm), and the BSi content per cell (c) and BSi/POC value (d) under 400 μatm and 1000 μatm with gradually rising (indicated as Gradually-T.p. or Gradually-T.w.) and directly rising CO_2 (indicated as Directly-T.p. or Directly-T.w.) in *Thalassiosira pseudonana* and *Thalassiosira weissflogii*. Samples for BSi measurement were collected in the middle of light phase. BSi ratio as a function of CO_2 concentration in *T. pseudonana* (open square, solid curve fit) and *T. weissflogii* (open circle, dashed curve fit) were fit with an exponential decay model; BSi/POC ratio as a function of CO_2 concentration in *T. weissflogii* (open circle, dashed curve fit) was fit with an exponential decay model. Dotted lines showed 95% confidence intervals. Different letters indicate significant difference between CO_2 treatments at $p < 0.05$ level; bars without labeling indicate no significant difference between CO_2 treatments.

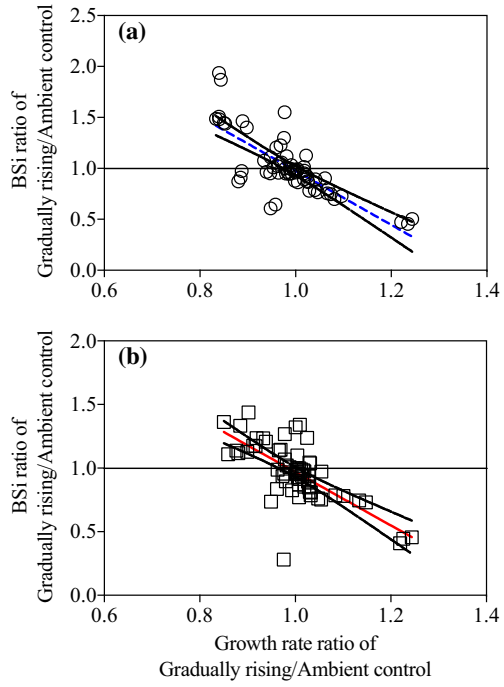

Fig. 9. The linear regression between BSi ratio and growth rate ratio of gradually rising CO_2 to ambient control in (a) *Thalassiosira pseudonana* (fitted equation: $y = -2.1 * x + 3.069$, $R^2 = 0.51$) and (b) *Thalassiosira weissflogii* (fitted equation: $y = -2.656 * x + 3.633$, $R^2 = 0.60$). BSi ratios and growth rate ratios presented in Figs. 8a and 2a.

from low to moderate CO_2 levels in both *T. pseudonana* and *T. weissflogii* indicate the silification process was significantly affected during the long-term process of simulated gradual OA. Si quota increased at low CO_2 levels (Milligan et al., 2004), and a lower growth rate will, all factors being equal, increase silicification due to the elongated cell cycle of G2 +M (Claquin et al., 2002). Decreased cellular BSi followed increased growth rates in both strains with gradually rising CO_2 (linear regression, $R^2 = 0.51$ and 0.60 in *T. pseudonana* and *T. weissflogii*, all $p < 0.0001$) (Fig. 9a, b). Therefore, increased growth rate with rising CO_2 may decrease BSi through changing the cell division cycle. Also, changes in extracellular pH could alter both the pH and carbonate chemistry in the exterior surface (Flynn et al., 2012) and also the intracellular acid base balance (Gao and Campbell, 2014). This changed pH homeostasis can affect silicon metabolism and therefore influence the frustule pattern formation, at least in *T. weissflogii* (Hervé et al., 2012). However, BSi did not further decrease from moderate to high CO_2 of 1000 μatm, which

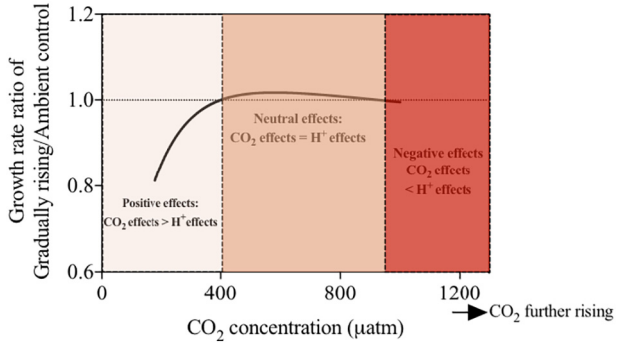

Fig. 10. A conceptual diagram of gradually rising CO_2/decreased pH effect on growth ratio of gradually rising CO_2 to ambient control treatments continuously grown under 400 μatm, based on this study. "CO_2 effect > H^+ effect" indicates positive effect (light pink background), "CO_2 effect = H^+ effect" indicates neutral effect (pink background), "CO_2 effect < H^+ effect" indicates negative effect (dark pink background). (For interpretation of the references to color in this figure legend, the reader is referred to the web version of this article.)

paralleled the pattern of growth rate across the two modulation methods.

Decreased biogenic silicate will cause silicon frustule attenuation and therefore changed optical properties which affect excitation capture and thus dissipation requirements (Ellegaard et al., 2016; Fuhrmann et al., 2004; Raven and Waite, 2004; Yamanaka et al., 2008). High CO_2 induced down-regulation of CCMs and the subsequent energy saving may further affect the photosynthetic performance if other potential stresses including light stress exist. Changing diatom silicate shells would also change carbon export through sedimentation to deep ocean (Tréguer et al., 2018). A decrease in Si/C ratio induced by high CO_2 was found in a bloom forming pennate diatom *Pseudonitzschia fraudulenta*, mainly due to increased cellular particulate organic carbon (Tatters et al., 2012). This changed Si/C was also found in the present study as BSi/POC decreased from low to moderate CO_2 levels in the larger cell of *T. weissflogii*, which means the function of larger diatom in biogeochemical cycle of both silicon and carbon, to some extent, may weaken, while the simultaneous decrease in cell volume may further intensify this effect by limiting sinking rate.

The elemental stoichiometry of POC to PON (C/N) may increase or not change under high CO_2 condition (Bellerby et al., 2008; Finkel et al., 2010; Riebesell et al., 2007; Van de Waal et al., 2010; Verschoor et al., 2013) and can be determined by interactive effects with other co-varied environmental factors (Gervais and Riebesell, 2001; Leonardos and Geider, 2005; Li et al., 2012). Decreased C/N with gradually rising CO_2 in the present study was due to the decrease of POC in both species. A decrease of C/N with rising CO_2 in *T. weissflogii* indicates the elemental stoichiometry of larger cell-size species affected more by high CO_2 and that the effects may be species specific.

The differential effects of gradually rising CO_2 vs. direct CO_2 shifts were most pronounced over low to moderate CO_2 levels. In contrast as CO_2 increased above current 400 μatm the modulation methods had limited effects on measured parameters. Ambient control showed some differences compared to 1000 μatm CO_2 whether achieved either directly or gradually. Carbon fixation rates decreased in gradually rising CO_2, while POC and PON decreased in directly rising CO_2 for *T. weissflogii*. The modulation method also had significantly differential effects on Chl a, carotenoid, NPQ and α in *T. pseudonana*, on growth rate, I_k and Si/C in *T. weissflogii*. Therefore, the differences between the CO_2 modulation methods appear to have significant implications on results and inferred conclusions. It is worth noting that in the present study we directly transferred the ambient culture (400 μatm) into 180 μatm, which was used as the starting point of gradual experiment after short term acclimation. Gradual adjustment of starting CO_2 level and even gradual transfer back from 1000 μatm to ambient level after a gradual rising CO_2 from 180 μatm may have generate further implications and to extend our understanding of acclimation and adaptation to OA.

It may be inappropriate to infer responses to gradual OA effects from comparisons of cell responses between ambient and a direct shift to high CO_2. The OA effects varied at different stages of acclimation time and CO_2 levels, especially from low to moderate CO_2 levels. Cell size of phytoplankton is important in the food chain, as the grazing activity by secondary producers is mainly size dependent (Frost, 1972) while the silicon frustule of diatoms may have significant mechanical protection against grazers (Hamm et al., 2003). OA dependent changes in cell size and silicon frustule, together with the changed elemental stoichiometry which determines nutrition value, may mediate grazing activity disproportionately across taxa, which will influence niche differentiation and ultimately alter the phytoplankton community structure and biogeochemical cycles.

Acknowledgement

This study was supported by National Natural Science Foundation of China (41720104005, 41721005, 31600317), and Joint Project of National

Natural Science Foundation of China and Shandong Province (No. U1606404), the China Postdoctoral Science Foundation (2015M582039) and Oversea Visiting Program for Universities and Colleges Youth Talents of Anhui Province (gxfx2017109). The funders had no role in study design, data collection and analysis, decision to publish, or preparation of the manuscript.

Author contributions

K.S.G. and W.L. designed the experiment. W.L., J.C.D., F.T.L., Y.L.Y., and T.F.W. performed the research. W.L., and K.S.G. analyzed the data. W.L., D.A.C. and K.S.G. wrote the manuscript, with contributions from all authors.

Appendix A. Supplementary data

Supplementary data to this article can be found online at https://doi.org/10.1016/j.scitotenv.2019.05.035.

References

Bellerby, R.G.J., Schulz, K.G., Riebesell, U., Neill, C., Nondal, G., Heegaard, E., et al., 2008. Marine ecosystem community carbon and nutrient uptake stoichiometry under varying ocean acidification during the PeECE III experiment. Biogeosciences 5, 1517–1527. https://doi.org/10.5194/bg-5-1517-2008.

Boyd, P.W., 2011. Beyond ocean acidification. Nat. Geosci. 4, 273–274. https://doi.org/10.1038/ngeo1150.

Boyd, P.W., Collins, S., Dupont, S., Fabricius, K., Gattuso, J.P., Havenhand, J., et al., 2018. Experimental strategies to assess the biological ramifications of multiple drivers of global ocean change-a review. Glob. Chang. Biol. 24, 2239–2261. https://doi.org/10.1111/gcb.14102.

Brennan, G., Collins, S., 2015. Growth responses of a green alga to multiple environmental drivers. Nat. Clim. Chang. 5, 892–897. https://doi.org/10.1038/nclimate2682.

Brzezinski, M.A., Nelson, D.M., 1995. The annual silica cycle in the Sargasso Sea near Bermuda. Deep-Sea Res. I Oceanogr. Res. Pap. 42, 1215–1237. https://doi.org/10.1016/0967-0637(95)93592-3.

Cai, W.-J., Hu, X., Huang, W.-J., Murrell, M.C., Lehrter, J.C., Lohrenz, S.E., et al., 2011. Acidification of subsurface coastal waters enhanced by eutrophication. Nat. Geosci. 4, 766–770. https://doi.org/10.1038/NGEO1297.

Caldeira, K., Wickett, M.E., 2003. Anthropogenic carbon and ocean pH. Nature 425, 365. https://doi.org/10.1038/425365a.

Capotondi, A., Alexander, M.A., Bond, N.A., Curchitser, E.N., Scott, J.D., 2012. Enhanced upper ocean stratification with climate change in the CMIP3 models. J. Geophys. Res. Oceans 117, C04031. https://doi.org/10.1029/2011JC007409.

Claquin, P., Martin-Jézéquel, V., Kromkamp, J.C., Veldhuis, M.J., Kraay, G.W., 2002. Uncoupling of silicon compared with carbon and nitrogen metabolisms and the role of the cell cycle in continuous cultures of *Thalassiosira pseudonana* (Bacillariophycea) under ligh, nitrogen and phosphorus control. J. Phycol. 38, 922–930. https://doi.org/10.1046/j.1529-8817.2002.t01-1-01220.x.

Collins, S., Rost, B., Rynearson, T.A., 2014. Evolutionary potential of marine phytoplankton under ocean acidification. Evol. Appl. 7, 140–155. https://doi.org/10.1111/eva.12120.

Cornwall, C.E., Hurd, C.L., 2015. Experimental design in ocean acidification research: problems and solutions. ICES J. Mar. Sci. 73, 572–581. https://doi.org/10.1093/icesjms/fsv118.

Doney, S.C., 2006. The dangers of ocean acidification. Sci. Am. 294, 58–65. https://doi.org/10.1038/ngeo1150.

Doney, S.C., Fabry, V.J., Feely, R.A., Kleypas, J.A., 2009. Ocean acidification: the other CO_2 problem. Annu. Rev. Mar. Sci. 1, 169–192. https://doi.org/10.1146/annurev.marine.010908.163834.

Ellegaard, M., Lenau, T., Lundholm, N., Maibohm, C., Friis, S.M.M., Rottwitt, K., et al., 2016. The fascinating diatom frustule-can it play a role for attenuation of UV radiation? J. Appl. Phycol. 28, 3295–3306. https://doi.org/10.1007/s10811-016-0893-5.

Feely, R.A., Sabine, C.L., Hernandez-Ayon, J.M., Ianson, D., Hales, B., 2008. Evidence for upwelling of corrosive "acidified" water onto the continental shelf. Science 320, 1490–1492. https://doi.org/10.1126/science.1155676.

Finkel, Z.V., Beardall, J., Flynn, K.J., Quigg, A., Rees, T.A.V., Raven, J.A., 2010. Phytoplankton in a changing world: cell size and elemental stoichiometry. J. Plankton Res. 32, 119–137. https://doi.org/10.1093/plankt/fbp098.

Flynn, K.J., Blackford, J.C., Baird, M.E., Raven, J.A., Clark, D.R., Beardall, J., et al., 2012. Changes in pH at the exterior surface of plankton with ocean acidification. Nat. Clim. Chang. 2, 510–513. https://doi.org/10.1038/nclimate1489.

Frost, B.W., 1972. Effects of size and concentration of food particles on the feeding behavior of the marine planktonic copepod *Calanus pacificus*. Limnol. Oceanogr. 17, 805–815. https://doi.org/10.4319/lo.1972.17.6.0805.

Fuhrmann, T., Landwehr, S., El Rharbi-Kucki, M., Sumper, M., 2004. Diatoms as living photonic crystals. Appl. Phys. B Lasers Opt. 78, 257–260. https://doi.org/10.1007/s00340-004-1419-4.

Gao, K., Campbell, D.A., 2014. Photophysiological responses of marine diatoms to elevated CO_2 and decreased pH: a review. Funct. Plant Biol. 41, 449–459. https://doi.org/10.1071/FP13247.

Gao, K., Helbling, E.W., Häder, D.P., Hutchins, D.A., 2012a. Responses of marine primary producers to interactions between ocean acidification, solar radiation, and warming. Mar. Ecol. Prog. Ser. 470, 167–189. https://doi.org/10.3354/meps10043.

Gao, K., Xu, J., Gao, G., Li, Y., Hutchins, D.A., Huang, B., et al., 2012b. Rising CO_2 and increased light exposure synergistically reduce marine primary productivity. Nat. Clim. Chang. 2, 519–523. https://doi.org/10.1038/nclimate1507.

Gao, K., Zhang, Y., Häder, D.-P., 2017. Individual and interactive effects of ocean acidification, global warming, and UV radiation on phytoplankton. J. Appl. Phycol. 30, 743–759. https://doi.org/10.1007/s10811-017-1329-6.

Gattuso, J.-P., Gao, K., Lee, K., Rost, B., Schulz, K.G., 2010. Approaches and tools to manipulate the carbonate chemistry. In: Riebesell, U., Fabry, V.J., Hansson, L., Gattuso, J.-P. (Eds.), Guide to Best Practices Ocean Acidification and Data Reporting. Publications Office of the European Union, Luxembourg, pp. 41–52 https://doi.org/10.1016/j.joms.2003.10.009.

Gattuso, J.-P., Magnan, A., Billé, R., Cheung, W.W., Howes, E.L., Joos, F., et al., 2015. Contrasting futures for ocean and society from different anthropogenic CO_2 emissions scenarios. Science 349, aac4722. https://doi.org/10.1126/science.aac4722.

Genty, B., Harbinson, J., Baker, N.R., 1990. Relative quantum efficiencies of the two-photosystems of leaves in photorespiratory and non-photorespiratory conditions. Plant Physiol. Biochem. 28, 1–10.

Gervais, F., Riebesell, U., 2001. Effect of phosphorus limitation on elemental composition and stable carbon isotope fractionation in a marine diatom growing under different CO_2 concentrations. Limnol. Oceanogr. 46, 497–504. https://doi.org/10.4319/lo.2001.46.3.0497.

Goldman, J.A., Bender, M.L., Morel, F.M., 2017. The effects of pH and pCO_2 on photosynthesis and respiration in the diatom *Thalassiosira weissflogii*. Photosynth. Res. 132, 83–93. https://doi.org/10.1007/s11120-016-0330-2.

Granum, E., Raven, J.A., Leegood, R.C., 2005. How do marine diatoms fix 10 billion tonnes of inorganic carbon per year? Can. J. Bot. 83, 898–908. https://doi.org/10.1139/b05-077.

Hamm, C.E., Merkel, R., Springer, O., Jurkojc, P., Maier, C., Prechtel, K., et al., 2003. Architecture and material properties of diatom shells provide effective mechanical protection. Nature 421, 841–843. https://doi.org/10.1038/nature01416.

Hennon, G.M.M., Quay, P., Morales, R.L., Swanson, L.M., Virginia Armbrust, E., 2014. Acclimation conditions modify physiological response of the diatom *Thalassiosira pseudonana* to elevated CO_2 concentrations in a nitrate-limited chemostat. J. Phycol. 50, 243–253. https://doi.org/10.1111/jpy.12156.

Hennon, G.M., Hernandez Limon, M.D., Haley, S.T., Juhl, A.R., Dyhrman, S.T., 2017. Diverse CO_2-induced responses in physiology and gene expression among eukaryotic phytoplankton. Front. Microbiol. 8, 2547. https://doi.org/10.3389/fmicb.2017.02547.

Hervé, V., Derr, J., Douady, S., Quinet, M., Moisan, L., Lopez, P.J., 2012. Multiparametric analyses reveal the pH-dependence of silicon biomineralization in diatoms. PLoS One 7, e46722. https://doi.org/10.1371/journal.pone.0046722.

Hönisch, B., Ridgwell, A., Schmidt, D.N., Thomas, E., Gibbs, S.J., Sluijs, A., et al., 2012. The geological record of ocean acidification. Science 335, 1058–1063. https://doi.org/10.1126/science.1208277.

Hopkinson, B.M., Dupont, C.L., Allen, A.E., Morel, F.M.M., 2011. Efficiency of the CO_2-concentrating mechanism of diatoms. Proc. Natl. Acad. Sci. U. S. A. 108, 3830–3837. https://doi.org/10.1073/pnas.1018062108.

Hutchins, D.A., Walworth, N.G., Webb, E.A., Saito, M.A., Moran, D., McIlvin, M.R., et al., 2015. Irreversibly increased nitrogen fixation in *Trichodesmium* experimentally adapted to elevated carbon dioxide. Nat. Commun. 6, 8155. https://doi.org/10.1038/ncomms9155.

Ihnken, S., Roberts, S., Beardall, J., 2011. Differential responses of growth and photosynthesis in the marine diatom *Chaetoceros muelleri* to CO_2 and light availability. Phycologia 50, 182–193. https://doi.org/10.2216/10-11.1.

Jin, P., Gao, K.S., Beardall, J., 2013. Evolutionary responses of a coccolothophorid *Gephyrocapsa oceanica* to ocean acidification. Evolution 67, 1869–1878. https://doi.org/10.1111/evo.1211210.5061/dryad.2ff80.

Key, T., McCarthy, A., Campbell, D.A., Six, C., Roy, S., Finkel, Z.V., 2010. Cell size trade-offs govern light exploitation strategies in marine phytoplankton. Environ. Microbiol. 12, 95–104. https://doi.org/10.1111/j.1462-2920.2009.02046.x.

Kroeker, K.J., Kordas, R.L., Crim, R., Hendriks, I.E., Ramajo, L., Singh, G.S., et al., 2013. Impacts of ocean acidification on marine organisms: quantifying sensitivities and interaction with warming. Glob. Chang. Biol. 19, 1884–1896. https://doi.org/10.1111/gcb.12179.

LaRoche, J., Rost, B., Engel, A., 2010. Bioassays, batch culture and chemostat experimentation. In: Riebesell, U., Fabry, V.J., Hansson, L., Gattuso, J.-P. (Eds.), Guide for Best Practices in Ocean Acidification Research and Data Reporting. Publications Office of the European Union, Luxembourg, pp. 81–94.

Leonardos, N., Geider, R.J., 2005. Elevated atmospheric carbon dioxide increases organic carbon fixation by *Emiliania Huxleyi* (Haptophyta), under nutrient-limited high-light conditions. J. Phycol. 41, 1196–1203. https://doi.org/10.1111/j.1529-8817.2005.00152.x.

Li, G., Campbell, D.A., 2013. Rising CO_2 interacts with growth light and growth rate to alter photosystem II photoinactivation of the coastal diatom *Thalassiosira pseudonana*. PLoS One 8, e55562. https://doi.org/10.1371/journal.pone.0055562.

Li, W., Gao, K., Beardall, J., 2012. Interactive effects of ocean acidification and nitrogen-limitation on the diatom *Phaeodactylum tricornutum*. PLoS One 7, e51590. https://doi.org/10.1371/journal.pone.0051590.

Li, W., Gao, K., Beardall, J., 2015. Nitrate limitation and ocean acidification interact with UV-B to reduce photosynthetic performance in the diatom *Phaeodactylum tricornutum*. Biogeosciences 12, 2383–2393. https://doi.org/10.5194/bg-12-2383-2015.

Li, F., Beardall, J., Collins, S., Gao, K., 2017a. Decreased photosynthesis and growth with reduced respiration in the model diatom *Phaeodactylum tricornutum* grown under

elevated CO_2 over 1800 generations. Glob. Chang. Biol. 23, 127–137. https://doi.org/10.1111/gcb.13501.
Li, W., Yang, Y., Li, Z., Xu, J., Gao, K., 2017b. Effects of seawater acidification on the growth rates of the diatom *Thalassiosira* (*Conticribra*) *weissflogii* under different nutrient, light, and UV radiation regimes. J. Appl. Phycol. 29, 133–142. https://doi.org/10.1007/s10811-016-0944-y.
Listmann, L., LeRoch, M., Schlüter, L., Thomas, M.K., Reusch, T.B., 2016. Swift thermal reaction norm evolution in a key marine phytoplankton species. Evol. Appl. 9, 1156–1164. https://doi.org/10.1111/eva.12362.
Lohbeck, K.T., Riebesell, U., Reusch, T.B.H., 2012. Adaptive evolution of a key phytoplankton species to ocean acidification. Nat. Geosci. 5, 346–351. https://doi.org/10.1038/ngeo1441.
Mejía, L.M., Isensee, K., Méndez-Vicente, A., Pisonero, J., Shimizu, N., González, C., et al., 2013. B content and Si/C ratios from cultured diatoms (*Thalassiosira pseudonana* and *Thalassiosira weissflogii*): relationship to seawater pH and diatom carbon acquisition. Geochim. Cosmochim. Acta 123, 322–337. https://doi.org/10.1016/j.gca.2013.06.011.
Milligan, A.J., Morel, F.M., 2002. A proton buffering role for silica in diatoms. Science 297, 1848–1850. https://doi.org/10.1126/science.1074958.
Milligan, A.J., Varela, D.E., Brzezinski, M.A., Morel, F.M., 2004. Dynamics of silicon metabolism and silicon isotopic discrimination in a marine diatomas a function of pCO_2. Limnol. Oceanogr. 49, 322–329. https://doi.org/10.4319/lo.2004.49.2.0322.
Morel, F.M.M., Rueter, J.G., Anderson, D.M., Guillard, R.R.L., 1979. Aquil: a chemically defined phytoplankton culture medium for trace metal studies. J. Phycol. 15, 135–141. https://doi.org/10.1111/j.1529-8817.1979.tb02976.x.
Nielsen, E.S., 1952. The use of radioactive carbon (C^{14}) for measuring organic production in the sea. ICES J. Mar. Sci. 18, 117–140. https://doi.org/10.1016/0140-6701(96)89406-9.
Parsons, T., Takahashi, M., 1973. Environmental control of phytoplankton cell size. Limnol. Oceanogr. 18, 511–515. https://doi.org/10.4319/lo.1973.18.4.0511.
Pelletier, G., Lewis, E., Wallace, D., 2007. CO_2Sys.xls: A Calculator for the CO_2 System in Seawater for Microsoft Excel/VBA. Washington State Department of Ecology/Brookhaven National Laboratory, Olympia, WA/Upton, NY, USA.
Platt, T., Gallegos, C., Harrison, W., 1980. Photoinhibition of photosynthesis in natural assemblages of marine phytoplankton. J. Mar. Res. 38, 687–701.
Raven, J., Waite, A., 2004. The evolution of silicification in diatoms: inescapable sinking and sinking as escape? New Phytol. 162, 45–61. https://doi.org/10.2307/1514475.
Reinfelder, J.R., 2011. Carbon concentrating mechanisms in eukaryotic marine phytoplankton. Annu. Rev. Mar. Sci. 3, 291–315. https://doi.org/10.1146/annurev-marine-120709-142720.
Richier, S., Achterberg, E.P., Humphreys, M.P., Poulton, A.J., Suggett, D.J., Tyrrell, T., et al., 2018. Geographical CO_2 sensitivity of phytoplankton correlates with ocean buffer capacity. Glob. Chang. Biol. 24, 4438–4452. https://doi.org/10.1111/gcb.14324.
Riebesell, U., Gattuso, J.-P., 2015. Lessons learned from ocean acidification research. Nat. Clim. Chang. 5, 12–14. https://doi.org/10.1038/nclimate2456.
Riebesell, U., Schulz, K.G., Bellerby, R.G.J., Botros, M., Fritsche, P., Meyerhöfer, M., et al., 2007. Enhanced biological carbon consumption in a high CO_2 ocean. Nature 450, 545–549. https://doi.org/10.1038/nature06267.
Ryckebosch, E., Muylaert, K., Eeckhout, M., Ruyssen, T., Foubert, I., 2011. Influence of drying and storage on lipid and carotenoid stability of the microalga *Phaeodactylum tricornutum*. J. Agric. Food Chem. 59, 11063–11069. https://doi.org/10.1021/jf2025456.
Sabine, C.L., Feely, R.A., Gruber, N., Key, R.M., Lee, K., Bullister, J.L., et al., 2004. The oceanic sink for anthropogenic CO_2. Science 305, 367–371. https://doi.org/10.1126/science.1097403.
Sarthou, G., Timmermans, K.R., Blain, S., Tréguer, P., 2005. Growth physiology and fate of diatoms in the ocean: a review. J. Sea Res. 53, 25–42. https://doi.org/10.1016/j.seares.2004.01.007.
Schaum, E., Rost, B., Millar, A.J., Collins, S., 2013. Variation in plastic responses of a globally distributed picoplankton species to ocean acidification. Nat. Clim. Chang. 3, 298–302. https://doi.org/10.1038/NCLIMATE1774.
Sett, S., Bach, L.T., Schulz, K.G., Koch-Klavsen, S., Lebrato, M., Riebesell, U., 2014. Temperature modulates coccolithophorid sensitivity of growth, photosynthesis and calcification to increasing seawater pCO_2. PLoS One 9, e88308. https://doi.org/10.1371/journal.pone.0088308.
Sunday, S., Qin, D., Manning, M., Chen, Z., Marquis, M., Averyt, K.B., et al., 2007. Climate change 2007: the Physical Science Basis. Contribution of Working Group I to the Fourth Assessment Report of the Intergovernmental Panel on Climate Change. Summ. for Policymakers. Intergov. Panel on Clim. Chang. 18, 95–123. https://doi.org/10.1016/S0925-7721(01)00003-7.
Sunday, J.M., Calosi, P., Dupont, S., Munday, P.L., Stillman, J.H., Reusch, T.B., 2014. Evolution in an acidifying ocean. Trends Ecol. Evol. 29, 117–125. https://doi.org/10.1016/j.tree.2013.11.001.
Tatters, A.O., Fu, F.-X., Hutchins, D.A., 2012. High CO_2 and silicate limitation synergistically increase the toxicity of *Pseudo-nitzschia fraudulenta*. PLoS One 7, e32116. https://doi.org/10.1371/journal.pone.0032116.
Thompson, P.A., Harrison, P.J., Parslow, J.S., 1991. Influence of irradiance on cell volume and carbon quota for ten species of marine phytoplankton. J. Phycol. 27, 351–360. https://doi.org/10.1111/j.0022-3646.1991.00351.x.
Tong, S., Gao, K., Hutchins, D.A., 2018. Adaptive evolution in the coccolithophore *Gephyrocapsa oceanica* following 1,000 generations of selection under elevated CO_2. Glob. Chang. Biol. 24, 3055–3064. https://doi.org/10.1111/gcb.14065.
Tréguer, P.J., De La Rocha, C.L., 2013. The world ocean silica cycle. Annu. Rev. Mar. Sci. 5, 477–501. https://doi.org/10.1146/annurev-arine-121211-172346.
Tréguer, P., Bowler, C., Moriceau, B., Dutkiewicz, S., Gehlen, M., Aumont, O., et al., 2018. Influence of diatom diversity on the ocean biological carbon pump. Nat. Geosci. 11, 27–37. https://doi.org/10.1038/s41561-017-0028-x.
Van de Waal, D.B., Verschoor, A.M., Verspagen, J.M., van Donk, E., Huisman, J., 2010. Climate-driven changes in the ecological stoichiometry of aquatic ecosystems. Front. Ecol. Environ. 8, 145–152. https://doi.org/10.1890/080178.
Verschoor, A.M., Van Dijk, M.A., Huisman, J., Van Donk, E., 2013. Elevated CO_2 concentrations affect the elemental stoichiometry and species composition of an experimental phytoplankton community. Freshw. Biol. 58, 597–611. https://doi.org/10.1111/j.1365-2427.2012.02833.x.
Webb, W.L., Newton, M., Starr, D., 1974. Carbon dioxide exchange of *Alnus rubra*. A mathematical model. Oecologia 17, 281–291. https://doi.org/10.2307/4215048.
Wellburn, A.R., 1994. The spectral determination of chlorophylls a and b, as well as total carotenoids, using various solvents with spectrophotometers of different resolution. J. Plant Physiol. 144, 307–313. https://doi.org/10.1016/S0176-1617(11)81192-2.
Wu, Y., Gao, K., Riebesell, U., 2010. CO_2-induced seawater acidification affects physiological performance of the marine diatom *Phaeodactylum tricornutum*. Biogeosciences 7, 2915–2923. https://doi.org/10.5194/bg-7-2915-2010.
Wu, Y., Campbell, D.A., Gao, K., 2014a. Faster recovery of a diatom from UV damage under ocean acidification. J. Photochem. Photobiol. B Biol. 140, 249–254. https://doi.org/10.1016/j.jphotobiol.2014.08.006.
Wu, Y., Campbell, D.A., Irwin, A.J., Suggett, D.J., Finkel, Z.V., 2014b. Ocean acidification enhances the growth rate of larger diatoms. Limnol. Oceanogr. 59, 1027–1034. https://doi.org/10.4319/lo.2014.59.3.1027.
Wu, Y., Campbell, D.A., Gao, K., 2017. Short-term elevated CO_2 exposure stimulated photochemical performance of a coastal marine diatom. Mar. Environ. Res. 125, 42–48. https://doi.org/10.1016/j.marenvres.2016.12.001.
Xu, J., Gao, K., Li, Y., Hutchins, D.A., 2014. Physiological and biochemical responses of diatoms to projected ocean changes. Mar. Ecol. Prog. Ser. 515, 73–81. https://doi.org/10.3354/meps11026.
Yamanaka, S., Yano, R., Usami, H., Hayashida, N., Ohguchi, M., Takeda, H., et al., 2008. Optical properties of diatom silica frustule with special reference to blue light. J. Appl. Phys. 103, 074701. https://doi.org/10.1063/1.2903342.
Yang, G., Gao, K., 2012. Physiological responses of the marine diatom *Thalassiosira pseudonana* to increased pCO_2 and seawater acidity. Mar. Environ. Res. 79, 142–151. https://doi.org/10.1016/j.marenvres.2012.06.002.
Zhang, Y., Bach, L.T., Lohbeck, K.T., Schulz, K.G., Listmann, L., Klapper, R., et al., 2018. Population-specific responses in physiological rates of *Emiliania huxleyi* to a broad CO_2 range. Biogeosciences 15, 3691–3701. https://doi.org/10.5194/bg-15-3691-2018.